Nanoscale

ROYAL SOCIETY OF CHEMISTRY

PAPER

View Article Online
View Journal | View Issue



Cite this: *Nanoscale*, 2025, **17**, 24601

# Chemistry of the shallow surface of isolated nanodiamonds probed by synchrotron X-ray photoemission

H. A. Girard, *[a] M. Finas,[a] L. Saoudi,[a] F. Ducrozet,[a,b] M. Briant,[a] O. Sublemontier,[a] A. R. Milosavljević,[c] C. Nicolas[c] and J.-C. Arnault[a]

Received 27th May 2025,
Accepted 18th September 2025

DOI: 10.1039/d5nr02241j

rsc.li/nanoscale

Nanodiamonds (NDs) are under active investigation for their unique properties and potential applications in energy harvesting, quantum technologies, and nanomedicine. The surface chemistry of NDs significantly influences their semiconducting behavior, colloidal properties, and interactions with water and light. To gain deeper insights into these properties, this study employs synchrotron X-ray photoelectron spectroscopy (XPS) to investigate the shallow surface chemistry of isolated nanodiamonds in an aerodynamic jet. Employing a photon energy of 360 eV, we probed the surface of nanodiamonds with a depth of 0.3 nm. Based on the collected data, the band diagrams of the nanoparticles have been established, reporting the expected differences in electron affinity between the two surface chemistries. Interestingly, both Ox-MNDs and H-MNDs showed fairly similar C 1s core level signatures, a phenomenon discussed in detail within the article, including the effect of residual water molecules. This raises important questions about the true interface formed with water molecules when NDs are in an aqueous suspension, particularly in the context of their use as photocatalysts.



## 1. Introduction

Nanoscale diamond particles, *i.e.* nanodiamonds (NDs), are currently under active investigation for their valuable and combinable properties in the fields of energy harvesting, quantum applications and nanomedicine.[1–3] Nanodiamonds inherit most of the outstanding properties of bulk diamond, in particular its semiconducting behavior in which surface chemistry plays a key role.[4] For instance, the diamond lattice linked to hydrogen atoms confers to hydrogenated nanodiamonds (H-NDs) a negative electron affinity (NEA), whereas oxygenated terminations (Ox-NDs) lead to a positive electron affinity (PEA).[5] The corresponding band diagram of hydrogenated nanodiamonds thus favors the emission of highly reducing solvated electrons under UV illumination, which have been successfully used for $CO_2$ or $N_2$ photocatalytic reduction[6,7] and more recently for pollutant degradation.[8,9] A p-type conductivity can also be obtained at the H-ND surface *via* interactions with adsorbates that act as electron acceptors through surface transfer doping.[5,10,11] The related electrical conductivity was measured for hydrogenated nanodiamonds of different natures and sizes.[12] Apart from influencing semiconducting properties, tuning the surface termination of nanodiamonds will also affect their colloidal behavior. NDs can be stabilized in water for months without any surfactant, but H-ND and Ox-ND aqueous suspensions will exhibit opposite surface charges with positive and negative zeta potentials at neutral pH, respectively.[13] If the cause of the negatively charged Ox-NDs is well known (carboxylate groups), the origin of the positive charge of H-NDs is still debated. Spectroscopic approaches[14,15] evidenced that surface chemistry influences the spatial arrangement of water molecules surrounding NDs. For H-NDs, these works suggested a long-range disruption of the water hydrogen bond network.

Still regarding the influence of surface chemistry on the physico-chemical properties of NDs, specific behaviors were observed considering light–matter interactions. For instance, aqueous colloids of hydrogenated nanodiamonds exposed to gamma or X-ray irradiation revealed unusual overproduction of hydroxyl radicals and/or solvated electrons compared to water radiolysis standards,[16–18] not reproduced for Ox-NDs. In contrast, photocatalytic hydrogen production *via* water splitting under visible light was only reported for oxidized NDs

[a]*Université Paris-Saclay, CEA, CNRS, NIMBE, 91191 Gif sur Yvette, France. E-mail: hugues.girard@cea.fr*
[b]*Institut de Chimie Physique, Université Paris-Saclay – CNRS, UMR 8000, 91405 Orsay, France*
[c]*Synchrotron SOLEIL, L'Orme des Merisiers Départementale 128, 91190 Saint-Aubin, France*

suspended in water.[19] The mechanisms involved in hydrogen production, including those taking place at the ND/water interface, are still unclear but are clearly specific to the oxidized surface.

Thus, to shed light on these specific properties of NDs in water according to their surface terminations, an investigation of their shallow surface chemistry is required to understand the real interface formed with water molecules when NDs are in a colloidal suspension. In that sense, X-ray photoelectron spectroscopy (XPS) appears to be an appropriate technique to study the surface chemistry of nanodiamonds.[20] Nevertheless, as the dimensions of the nanoparticles approach the inelastic mean free path (IMFP) of the generated photoelectrons (which is a few nanometers in diamond), conventional XPS data must be carefully analyzed to account for so-called "nano-effects": the signal from the surface may become predominant depending on the size of the nanoparticles.[21–23] To mitigate this effect, a smaller IMFP should be considered, as previously performed on bulk diamond.[24,25] Another limitation of conventional XPS is the deposition of nanoparticles on a substrate. Depending on the contact between the nanodiamonds (NDs) and the underlying layer, inhomogeneous surface charging can occur during analysis, which can distort both the appearance of the core-level photoemission peaks and their binding energy positions. This aspect is particularly crucial when comparing hydrogenated NDs, which are conductive,[11] with oxidized NDs, which are highly insulating.

In this context, this article aims to describe XPS analysis performed on a jet of isolated (or slightly aggregated) nanodiamonds, directly produced from an aqueous colloid through a nebulizer and an aerodynamic lens.[26,27] Using a synchrotron photon beam that intersects the jet of nanoparticles, photoelectrons coming from isolated NDs were then analyzed in terms of energy. To probe the shallow surface of the nanoparticles, a photon energy of 360 eV was used, unless specified otherwise, which corresponds to an inelastic mean free path (IMFP) estimated to be 0.3–0.5 nm for C 1s electrons in diamond.[28,29] By employing a nanoparticle jet instead of a substrate deposit, it was thus possible to circumvent charging effects. In this study, we focused on the surface chemistry of hydrogenated and oxidized nanodiamonds synthesized through a milling process,[30] as their electronic properties closely resemble those of bulk diamond.

## 2. Results

The XPS analyses presented below were performed on milled nanodiamonds (MNDs) that were oxidized (Ox-MNDs) or hydrogenated (H-MNDs) in gas phase at high temperature, following procedures detailed in our previous studies.[10,11] Thus, for complete characterization of these H-MNDs and Ox-MNDs, including dynamic light scattering experiments and infrared or Raman spectroscopy techniques, please refer to our previous paper.[10]

### Hydrogenated MNDs

Fig. 1(a) shows the C 1s XPS spectrum of H-MNDs recorded for a photon energy of 360 eV. Binding energies are referenced here to the vacuum level defined with $CO_2$ gas introduced into the UHV chamber which serves as a reference ($E_B$ = 297.65 eV).[31]

Under these conditions, the C 1s peak maximum of the H-MND nanoparticles is located at 288.6 eV.

In order to gain further insight into this spectrum, deconvolution and assignment of the components are mandatory, but it is important to keep in mind that at this photon energy, only the very first atomic layers are probed. There is currently no assurance that the predominant peak aligns with the signature of diamond C–C $sp^3$ bonds, which would allow the attribution of the other peaks. A comparative analysis with the C 1s spectrum recorded using a conventional spectrometer, *i.e.*,

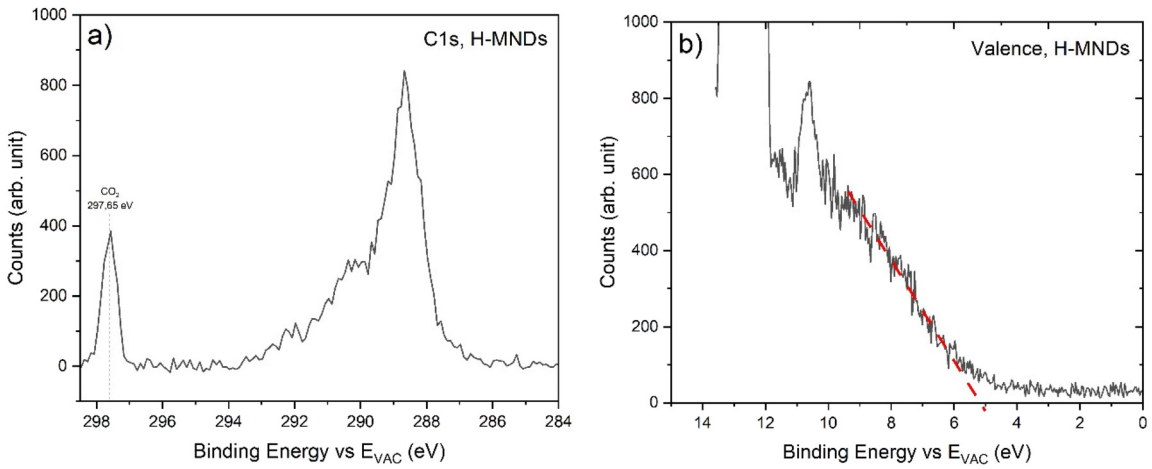


**Fig. 1** Photoelectron spectra of hydrogenated milled NDs. (a) C 1s spectrum recorded with a photon energy of 360 eV. (b) Valence band spectrum recorded with a photon energy of 100 eV. At photon energies of 360 eV and 100 eV, the overall resolutions in the XPS spectra were 0.39 and 0.11 eV, respectively. Binding energies are referenced to the vacuum level defined with $CO_2$ gas.

 

a standard laboratory spectrometer equipped with a monochromatic Al Kα (1486.6 eV) X-ray source, is thus proposed. However, a straightforward comparison of both C 1s spectra is impossible, as the binding energies obtained using a conventional spectrometer are referenced to the Fermi level of the material ($E_F$), whereas in the experiments carried out with the synchrotron beam using a nanoparticle jet, the energies are referenced to $E_{VAC}$ given by the isolated $CO_2$ molecules that serve as a reference (see the Methods section). Note that in our nanoparticles, it would be more appropriate to consider a near-surface vacuum level, which corresponds to the energy level of an electron with zero kinetic energy relative to the sample surface ($E_{VAC}(s)$), distinct from the vacuum level at infinity ($E_{VAC}(\infty)$), which represents the energy of an electron at rest far from the solid surface.[32] In XPS/UPS measurements, this $E_{VAC}(s)$ should be considered to build a band diagram. However, due to the specificity of the measurement performed here, conducted on isolated nanoparticles that are not in contact with a substrate, this local vacuum level cannot be strictly defined; only the($E_{VAC}(\infty)$ derived from $CO_2$ gas is available.

To overcome this issue, referring both C 1s spectra to the maximum of the valence band ($E_{VBM}$) would allow reliable comparison. Fig. 1(b) shows the valence band spectrum recorded for H-MNDs with the synchrotron beam, referenced to $E_{VAC}$, derived from $CO_2$ gas. A maximum of the valence band at 5.1 eV was measured. With a conventional XPS approach, a value of 1.1 eV *vs.* $E_F$ was previously measured for similar H-MNDs.[10] According to these values, a simplified band diagram is proposed in Fig. 2(a). Thanks to the synchrotron measurements, the valence band maximum of H-MNDs can be positioned at 5.1 eV below the $E_{VAC}$. From conventional XPS results, the Fermi level of the material ($E_F$) can be positioned at 1.1 eV above the valence band maximum. The C 1s maximum of conventional and synchrotron measurements can then be reported at 284.8 eV *vs.* $E_F$ and 288.6 eV *vs.* $E_{VAC}$ respectively. By adopting the valence band maximum ($E_{VBM}$) as a new common reference, it appears that the two C 1s maxima are nearly identical, both positioned at 283.6 eV, within the margin of experimental error. This simplified band diagram further evidences that, if we consider a band gap of 5.4 eV previously measured by reflection electron energy loss spectroscopy (REELS) for the same nanoparticles,[11] a similar negative electron affinity (0.3 eV) to the one measured by UPS in earlier reports is obtained.[5,11] This evidences that the vacuum level derived from the calibration gas is close to the local $E_{VAC}$ of the nanoparticles, within the margin of experimental error.

The C 1s spectra obtained using the synchrotron and the conventional spectrometers are shown in Fig. 2(b), both referenced to the $E_{VBM}$. Note that the energy resolution of the conventional spectrometer for a C 1s spectrum under our analysis conditions is around 0.35 eV, which is the same order of magnitude as that for synchrotron XPS. This allows the comparison made here.

Considering the agreement in the position of the C 1s peak and the similar energy resolutions of the two spectrometers, we thus applied to both spectra the fitting parameters previously reported for the conventional XPS analysis.[10] Fitted spectra are presented in Fig. 3. The energy position and relative area of each contribution are presented in Table 1.

In both cases, the main peak corresponds to the C–C $sp^3$ bonds of diamond. The second contribution at higher binding energy (+0.7 eV) can be assigned to defective C–C $sp^3$ bonds, including core and surface defects of the diamond lattice, as well as $sp^3$ carbons in the vicinity of surface terminations. It is important to highlight here that hydrogenated surface termin-

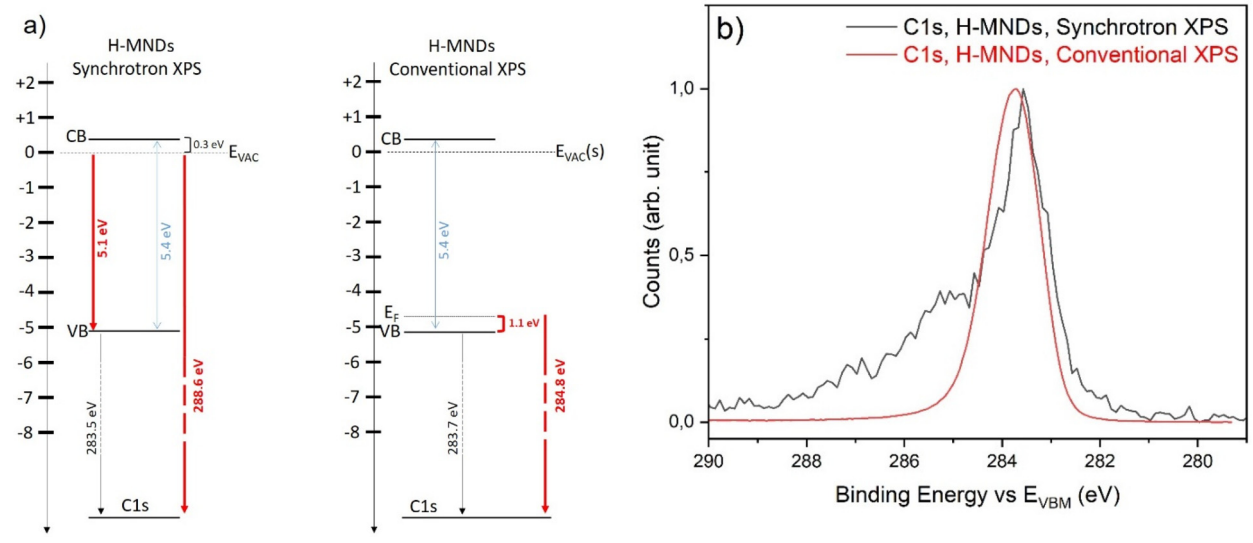


**Fig. 2** (a) Simplified band diagrams of H-MNDs built from synchrotron and conventional XPS measurements (red) and values from the literature (blue) and (b) C 1s spectra of H-MNDs recorded on synchrotron and conventional XPS. The spectra are normalized to the main contribution. Binding energies are referenced to the $E_{VBM}$.

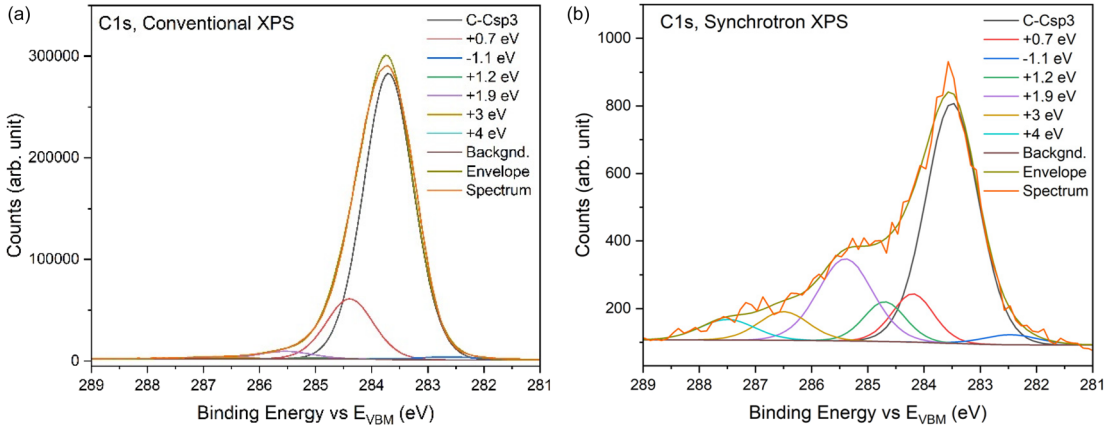


**Fig. 3** C 1s-fitted spectra of H-MNDs recorded on (a) conventional and (b) synchrotron XPS. Binding energies are referenced to the $E_{VBM}$.

**Table 1** Details of the different contributions of the C 1s-fitted spectra of H-MNDs and their relative area (in %) for conventional and synchrotron XPS

| | | C 1s relative area (%) | |
|---|---|---|---|
| Assignments | Energy shift (eV) | Conv. XPS | Synch. XPS |
| C=C $sp^2$ | −1.1 eV | 1.0 | 2.3 |
| C–C $sp^3$ | C–C $sp^3$ | 79.9 | 52.9 |
| C–C defects | +0.7 eV | 15.9 | 8.4 |
| C–OH | +1.2 eV | 0.3 | 6.9 |
| C–O–C | +1.9 eV | 2.2 | 18.9 |
| C=O | +3 eV | 0.6 | 6.0 |
| COOH | +4 eV | 0.1 | 4.6 |

ations, *i.e.*, surface carbon atoms saturated with one or several hydrogen atoms, will not be directly visible by XPS but their presence will contribute to this defective C–C component.[33,34] The four other peaks at higher binding energies are related to oxygen functional groups with C–OH, C–O–C, C=O and COOH bonds at +1.2, +1.9, +3 and +4 eV, respectively.[10,35] The peak recorded at lower binding energy (−1.1 eV) corresponds to C=C $sp^2$ bonds.

As the shallow surface is highly overexpressed with synchrotron XPS, we can note a significant decrease of the "bulk" contributions, the C–C $sp^3$ bonds and that related to defects, from 80% to 53% and from 16% to 8%, respectively. At the same time, contributions related to functional oxygen groups are all enhanced, from 3% to 37% in total. The important proportion of carbon–oxygen functions at the surface of H-MNDs will be discussed later.

Considering the peak related to $sp^2$ C=C bonds, the contributions measured at 360 eV (synchrotron XPS) and 1486 eV (conventional XPS) remain very close and very limited (<2.5% of the total C 1s area). Such bonds may result from local reconstructions of unsaturated carbon bonds after the hydrogenation gas treatment.[35] However, given that this component is related to the surface of the nanoparticles, it is surprising that it does not increase when lowering the photon energy.

### Oxidized-MNDs

For Ox-MNDs, the C 1s maximum is located at 291 eV with a FWHM of 2 eV (Fig. 4(a)). This peak appears significantly wider than the one obtained for H-MNDs (Fig. 1). Fig. 4(b) shows the valence band spectrum recorded for Ox-MNDs with a maximum at 6.9 eV *vs.* $E_{VAC}$. With a conventional XPS approach, a value of 3.4 eV *vs.* the Fermi level ($E_F$) was previously measured for similar Ox-MNDs.[10] Consequently, a band diagram built from these information is shown in Fig. 5(a). Here, a difference of 0.4 eV is obtained between the C 1s maxima recorded using the synchrotron and that using conventional spectrometers. These band diagrams also reveal a positive electron affinity (PEA) of 1.5 eV, which is expected for Ox-MNDs.[5,11]

As for H-MNDs, conventional and synchrotron XPS spectra were rescaled to the $E_{VBM}$ and are displayed in Fig. 5(b).

We applied to both spectra the fitting previously reported for conventional XPS analysis.[10] Fitted spectra are presented in Fig. 6. The position and relative area of each contribution are presented in Table 2.

As the shallow surface is highly preferentially probed at 360 eV (synchrotron), we can note a significant decrease of the C–C $sp^3$ bulk contribution from 76% to 28%. As for H-MNDs, all contributions related to carbon–oxygen groups are enhanced: from 9% to 40% in total. The C=C $sp^2$ contribution shows a significant increase from 4% to 11% of the total C 1s area. For Ox-MNDs, the contribution related to defects (+0.7 eV *vs.* C–C $sp^3$) is increased from 11 to 21%. This would suggest a higher density of defects at the surface compared to H-MNDs (in agreement with HRTEM observations[10]).

## 3. Discussion

In recent years, there has been a growing interest in nanodiamonds produced by milling (MNDs), with a focus on their surface chemistry, electronic properties, and colloidal behavior. The prevailing consensus is that these MNDs exhibit sig-

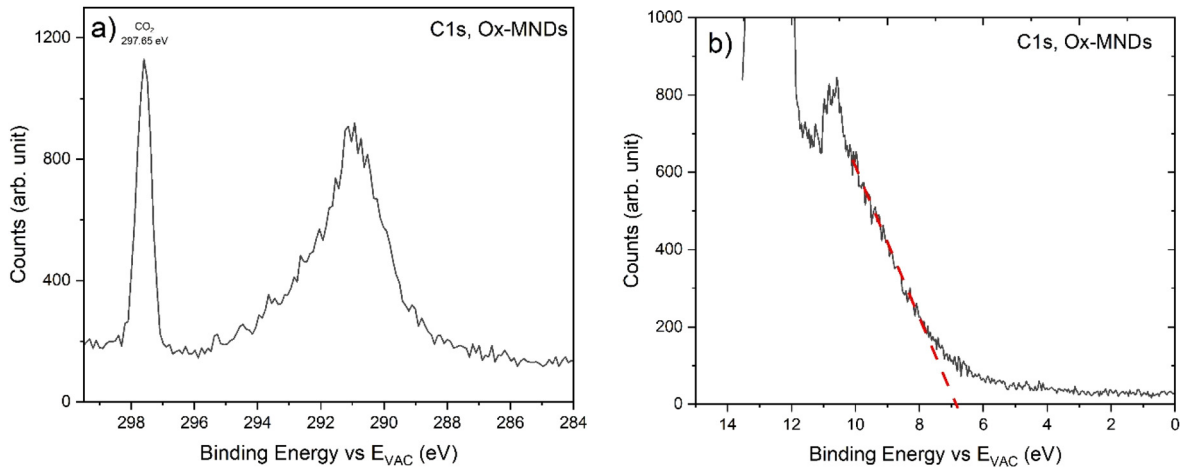


**Fig. 4** (a) C 1s spectra of oxidized milled NDs (Ox-MNDs) and the $CO_2$ reference recorded with a photon energy of 360 eV. (b) Valence band spectrum of Ox-MNDs recorded with a photon energy of 100 eV. Binding energies are referenced to the vacuum level defined with $CO_2$ gas.

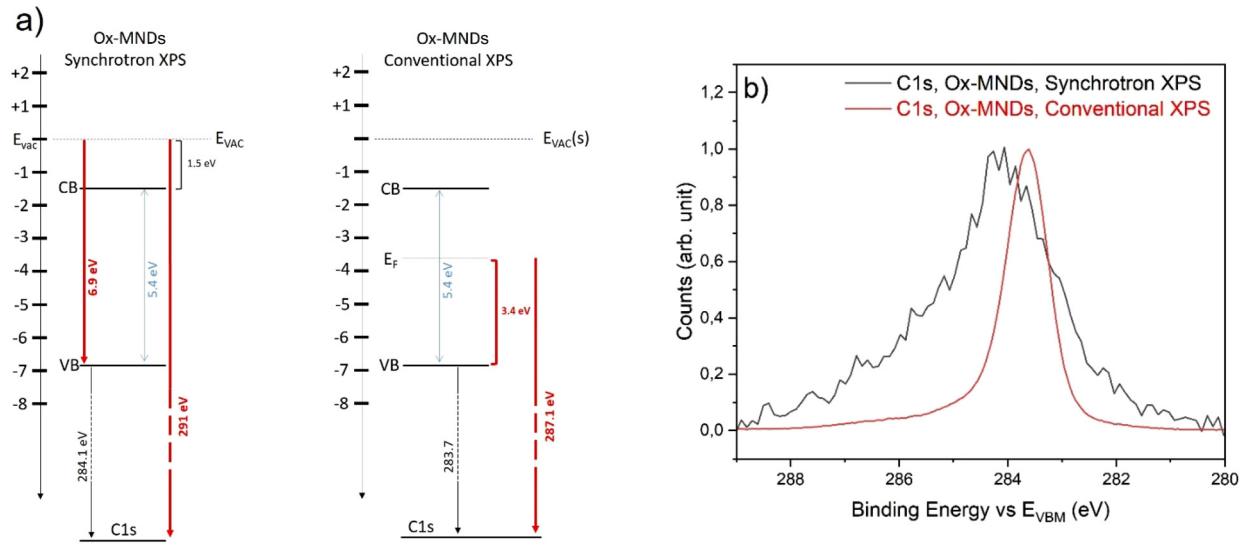


**Fig. 5** (a) Simplified band diagrams of Ox-MNDs built from synchrotron and conventional XPS measurements (in red) and values from the literature (in blue) and (b) C 1s spectra of Ox-MNDs recorded on synchrotron and conventional XPS. Spectra are normalized in intensity to the main carbon contribution. Binding energies are referenced to the $E_{VBM}$.

nificant similarities to bulk diamond, especially in their surface chemistry and electronic properties. This originates from their excellent crystalline quality. For instance, IR, Raman and photo-electron spectroscopy analyses of Ox-MNDs show an oxidized chemistry composed of alcohols, ethers, carbonyl groups and carboxyl groups, similar to that seen for bulk diamond.[7,10,36,37] It should be noted that a residual $sp^2$ carbon is also generally measured for these Ox-MNDs. In contrast, H-MNDs, which are typically obtained by annealing Ox-MNDs under $H_2$ at temperatures higher than 700 °C,[7,10,36] exhibit a nearly complete desorption of oxidized functions, accompanied by a decrease in $sp^2$ carbon.[10,36] In a similar manner to bulk hydrogenated diamond, a surface conductivity has been demonstrated by several research groups on these H-MNDs, either indirectly by infrared spectroscopy *via* Fano-type destructive interferences[36,38,39] or more directly by conductivity measurements.[12] Recent UPS/XPS studies conducted by our team have also revealed that this conductivity can likely be attributed to adsorbates originating from air and/or water, which induce a pseudo p-type behavior *via* a charge transfer mechanism.[11] Furthermore, we have demonstrated the feasibility of inducing and removing this pseudo p-type doping by exposing the sample to vacuum annealing and re-exposure to water/air.

However, most of the spectroscopic studies cited above that have been used in recent years to investigate the chemical and semiconducting properties of H-MNDs and Ox-MNDs were carried out on nanoparticles that were drop-cast or spin-coated

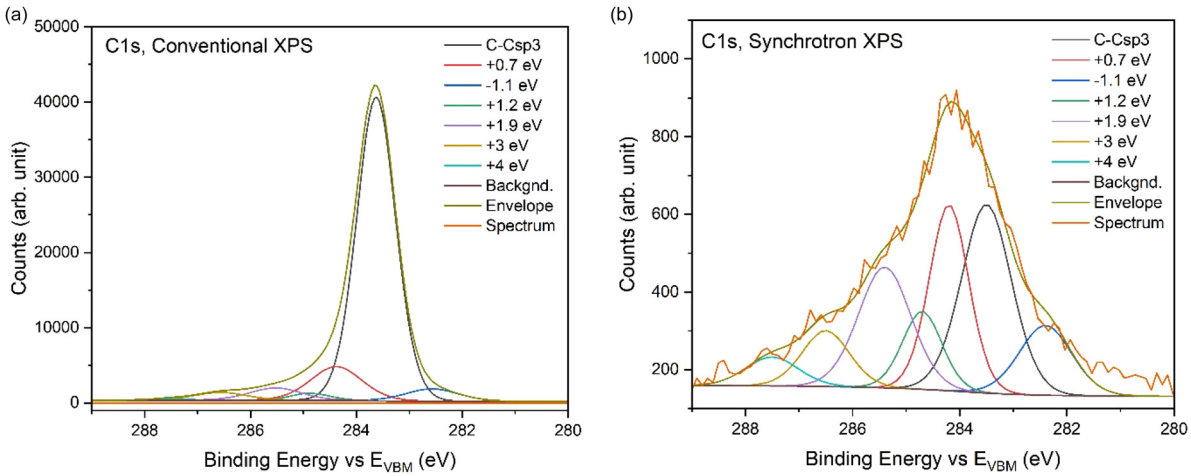


Fig. 6 C 1s-fitted spectra of Ox-MNDs recorded on (a) conventional and (b) synchrotron XPS. Binding energies are referenced to the $E_{VBM}$.

Table 2 Details of the different contributions of the C 1s-fitted spectra of Ox-MNDs and their relative area (in %) for conventional and synchrotron XPS

| | | C 1s relative area (%) | |
|---|---|---|---|
| Assignments | Energy shift (eV) | Conv. XPS | Synch. XPS |
| C=C $sp^2$ | −1.1 eV | 4.0 | 10.7 |
| C–C $sp^3$ | C–C $sp^3$ | 76.1 | 27.9 |
| C–C defects | +0.7 eV | 11.1 | 21.4 |
| C–OH | +1.2 eV | 1.7 | 9.0 |
| C–O–C | +1.9 eV | 4.1 | 18.7 |
| C=O | +3 eV | 2.6 | 7.8 |
| COOH | +4 eV | 0.4 | 4.5 |

on a substrate from a colloidal suspension. This methodological approach, mandatory for analyzing nanoparticles with conventional tools, may not accurately reflect the surface chemistry of nanodiamonds as they exist in colloids. Depositing a drop of solvent containing nanoparticles and then allowing it to dry can potentially alter their surface chemistry, particularly with regard to adsorbates, as well as promoting strong interactions with the substrate during spectroscopic measurements.[40] Finally, with specific regard to XPS, it is important to remember that while this technique is rightly considered as surface analysis for bulk materials, it differs at the scale of nanometric particles. As briefly mentioned in the introduction, at the energies usually employed in laboratory spectrometers (Al Kα: 1486.6 eV), electron escape depths are of the order of a few nanometers for diamond.[29] Given the wide size distribution of MNDs,[41] which ranges from a few nanometers to a few dozen, the collected photoelectrons may originate either from the core for the smallest nanoparticles or from the surface for the largest nanoparticles. Additionally, for the smallest nanoparticles (<10 nm), an enhancement of the surface contribution may also arise, as clearly established by Baer *et al.*[21]

The results presented here have therefore the advantage of being truly "surface sensitive", even at the scale of nanoparticles, since we probe mostly 0.3–0.5 nm beneath the surface. Furthermore, this approach using a jet allows the nanoparticles to statistically receive not more than one photon each,[42] thus X-ray-induced surface modification can be avoided, thereby ensuring even more reliable results. Therefore, we have access to the real signature of the surface chemistry of MNDs, as close as possible to what they are in colloids, with no risk of distortion of the XPS spectra due to interaction with a substrate, a charging effect or even *in situ* modification under X-rays.

Considering all these factors, we can now compare accurately the surface chemistries of H-MNDs and Ox-MNDs. For Ox-MNDs, an enhancement of surface-related functions (carbon–oxygen groups and $sp^2$ carbon) and sub-surface functions (defective $sp^3$ C–C bonds) is observed compared to conventional XPS analysis, with a concomitant reduction of the core component (C–C $sp^3$). This finding is consistent with prior studies employing energy-resolved XPS on bulk diamond, which demonstrated an enhancement of surface components for photon energies close to 360 eV.[24,43] In their study, Chemin *et al.* reported a C 1s core level of oxidized bulk diamond recorded with a photon energy of 335 eV (IMFP ≈ 0.6 nm), where the core component accounted for approximately 60% of the total carbon, without distinguishing between the C–C $sp^3$ and defective $sp^3$ C–C bonds. Here, the combined contribution of C–C $sp^3$ and defective $sp^3$ C–C bonds reaches nearly 50% of the carbon, which is of the same order of magnitude.

In contrast, the surface analysis of H-MNDs presents a more challenging aspect to address. Compared to Ox-MNDs, the C–C $sp^3$ component is the main one related to the nanoparticle core. This is due to the reduced presence of defective C–C bonds and $sp^2$ carbon bonds. This observation aligns with previous reports where annealing under $H_2$ of oxidized surfaces has been shown to "heal" the surface defects and remove residual $sp^2$ carbon.[10,35]

Another notable finding is the presence of "carbon–oxygen" related groups in the C 1s spectrum of H-MNDs, with

 

proportions nearly identical to those observed for Ox-MNDs (37% of the overall C 1s for H-MNDs *versus* 40% for Ox-MNDs). Examining the O 1s spectra recorded for H-MNDs and Ox-MNDs, as shown in Fig. 7, it appears that both MNDs are covered with a water layer (539.8 eV), with no obvious other contributions. Note that due to the geometry of the system, we can ensure that this XPS signal is related to the surface of nanodiamonds and is not originating from the carrier gas and the residual solvent.[45] While these O 1s spectra do not provide information about O–C components, which should be hidden by the water signature, they highlight the high affinity of H-MNDs for water.

The origin of these apparent C–O and C=O signatures on the C 1s core level of H-MNDs is a crucial aspect to investigate. IR spectroscopy and conventional XPS highlight clear differences in surface chemistries between H-MNDs and Ox-MNDs, as revealed in our previous study of nanodiamonds prepared under identical conditions.[10] Briefly, Ox-MNDs contained over 9 at% oxygen, as measured by conventional XPS, with strong C=O stretching modes in their IR spectrum. In contrast, H-MNDs exhibited only 1 at% oxygen, showing in their IR spectrum a near-complete disappearance of C=O modes, replaced by strong C–H stretching modes. However, these techniques either analyze the entire nanoparticle (IR) or account for a variable portion of the core (XPS, as explained above). As a result, the surface chemistry may be masked by contributions from sub-surface or core regions. Nevertheless, if the H-MND surface was truly oxidized, with a similar proportion of oxidized terminations to that in Ox-MNDs, it would contradict the electron affinity measurements. These measurements show a clear shift from positive for Ox-MNDs (+1.5 eV) to negative for H-MNDs (−0.3 eV), as determined from the position of the $E_{VBM}$.[10] It is therefore obvious that there is an apparent incoherence between equivalent proportions of C–O/C=O terminations as measured in the C 1s spectra of Ox-MNDs and H-MNDs, while two clearly distinct signs and values of the electron affinity are simultaneously observed. As recently reviewed by Hamers' team, the negative electron affinity (NEA) is directly linked to the presence of H-terminations and the associated $C^{\delta-}$–$H^{\delta+}$ surface dipoles, while the positive electron affinity is linked to oxidized terminations ($C^{\delta+}$–$O^{\delta-}$).[24] Therefore, two diamond materials evidencing such different electron affinities (in signs and values) should exhibit very significant differences in terms of the proportion of carbon–oxygen functions at their surface.[46]

At this stage, only hypotheses can be advanced to clarify this apparent contradiction. One can assume first a different spatial location of C–O bonds at both MND surfaces, within the first nanometer of the nanoparticles. Such oxygen functional groups may be present at the surface of H-MNDs, while it may be partially covered by the more abundant $sp^2$ carbon for Ox-MNDs (Table 2). Such a hypothesis may lead to an underestimation of C–O bonds for the oxidized surface in the present XPS analysis, which mainly probes the shallow surface at 360 eV. This hypothesis would explain the different evolutions of carbon–oxygen contributions for a higher probed depth (at 580 eV): a clear decrease for H-MNDs (Fig. 8) and an unchanged signal for Ox-MNDs (Fig. 8). However, for MNDs, we have no other experimental evidence to support such surface structuring.

Another possibility would be to consider that C–O and C=O components may not be linked to carbon–oxygen groups covalently bonded to the MND surface, but may originate from some species adsorbed on their surface, which would not affect the NEA. This postulate is supported by the C 1s spectrum recorded at a higher photon energy of 580 eV for H-MNDs, which allows us to probe a little deeper into the particle (up to 0.6 nm). As shown in Fig. 8(a), the shoulder at 290.5 eV, which would correspond to the signature of these species adsorbed on the H-MND surface, is less pronounced at

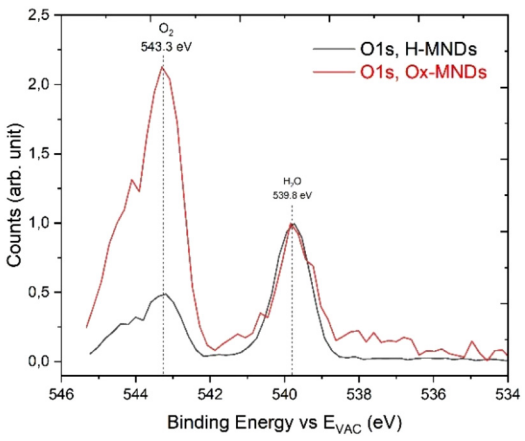


**Fig. 7** O 1s spectra of H-MNDs and Ox-MNDs recorded at 600 eV, referred to the $E_{VAC}$. The spectra are normalized to the 539.8 eV peak. $O_2$ gas was introduced into the UHV chamber as a binding energy reference (543.3 eV).[44]

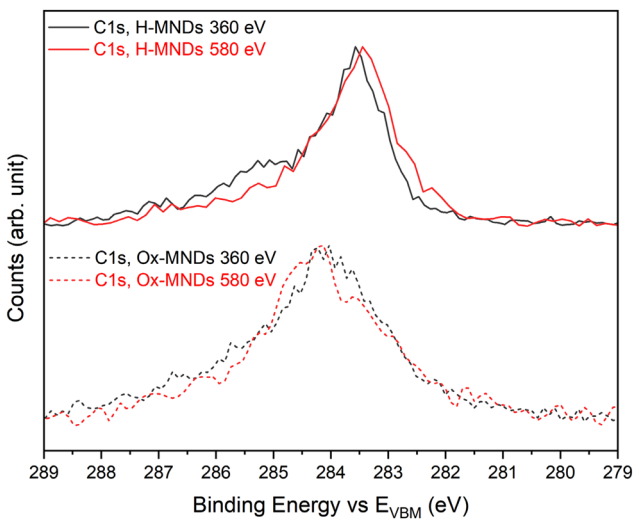


**Fig. 8** C 1s spectra of H-MNDs and Ox-MNDs recorded at 360 eV and 580 eV. The spectra are normalized to the main contribution. Binding energies are referenced to the $E_{VBM}$.

higher photon energies. At this stage, it is important to remember that these experiments reflect as closely as possible the state of the nanoparticles as they are in the colloid, without any interaction with a substrate. In the present experiment, nanoparticles are nebulized from the colloid for a few fractions of a second before being analyzed, and they only dry for a very short time. As a matter of fact, they remain surrounded by a thin water layer during the analysis, as shown by the O 1s spectrum (Fig. 7), on which a water signature is clearly visible at 539.8 eV.[44] This water layer lying at the surface of H-MND may also participate to the significant presence of C–O/C═O terminations on their surface. Over the last two decades, numerous theoretical and experimental studies have explored the spontaneous interactions between water and hydrogenated bulk diamond surfaces.[47–49] These studies suggest that the dissociation of water molecules is likely to occur on both hydrogenated and bare diamond surfaces, a process facilitated by carbon dimers and dangling bonds. In some cases, the dissociation of water molecules on a diamond surface can result in the formation of weakly bound carbonyl and alcohol groups.[48] The observed phenomenon may involve the formation of weakly bound C–O/C═O terminations upon contact with water, potentially located on dangling bonds and reconstructed surfaces, while the negative electron affinity due to the C–H terminations remains preserved. It should be noted that in the work of Chemin *et al.*,[43] the C 1s core levels of hydrogenated bulk diamond surfaces, also characterized using a photon energy of 335 eV, do not exhibit such C–O and C═O functionalities. This is likely because a water layer is not expected to be preserved in these experiments, which are performed under ultra-high vacuum conditions and on surfaces that have only been exposed to ambient air beforehand.

Addressing the potential existence of a chemical compound lying at the surface of the H-MNDs, it is also essential to consider recent research works that have revealed their surface conductivity[10,12,38,39] and the pseudo p-type doping that we measured by UPS experiments on the same H-MNDs.[11] This was also reported for an equivalent material in the work of Miliaieva *et al.*[5] This pseudo p-type doping originates from a transfer doping mechanism, which requires the presence of electron acceptors located at the surface. In the context of bulk diamond, molecular species such as $O_3$, $NO_2$, NO, and $SO_2$ have been postulated and studied as electron acceptors, resulting in surface conductivity even at very low concentrations.[4] In our previous study, we hypothesized that $NO_3^-$, $NO_2^-$ and/or $O_3$ may be responsible for the pseudo p-type doping observed in these H-MNDs.[11] However, these species would not participate in the C 1s signature of the shallow surface of H-MNDs. Focusing on carbon-based adsorbates involved in charge transfer doping, in their pioneering works during the 2000s,[50,51] Maier, Ristein and co-workers demonstrated that $HCO_3^-$ anions originating from $CO_2$ were dissolved in the adsorbed water layer at the diamond surface. They proposed that $HCO_3^-$ anions could be present at the diamond surface to compensate for the positive charge of the $h^+$ layer. Nevertheless, according to the NIST database and the literature,[52] the C 1s signature of $HCO_3^-$ anions adsorbed on thin film oxides should be located at binding energies ranging from 289 to 292 eV *vs.* $E_F$. Here is the limit of this hypothesis, as we lack information on the binding energies of such anions adsorbed on nanodiamonds or nanocarbons, referenced to the $E_{VAC}$.

Another possibility concerns the presence of adventitious carbon at the surface of MNDs. Thanks to the use of a nanoparticle jet directly formed from the colloid, the usual contamination occurring during the exposure of drop-casted particles to ambient atmosphere throughout their preparation and storage is avoided here. However, when preparing the colloid, the nanoparticles were necessarily exposed to air between the time they left the oven and the time they were introduced into the ultrapure water for sonication. Under our experimental conditions, this exposure to ambient air lasts a few hours up to a few days at maximum, during which we cannot exclude that a small amount of adventitious carbon is deposited on the surface of the powder. In 2017, Greczynski *et al.*[53] studied this adventitious carbon on different types of thin films (metal, nitride, carbide, boride, oxide, and oxynitride) and measured a constant binding energy of 289.6 eV *vs.* $E_{VAC}$ whatever the substrate.[54] Considering our C 1s spectra, this binding energy seems a little lower than that of the C–O and C═O components. Thus, if we cannot exclude a contribution of this incidental carbon, it will remain limited and anyway it does not prevent the demonstration of negative electronic affinity (NEA) on H-MNDs and positive electronic affinity (PEA) for Ox-MNDs.

## 4. Conclusion

Better knowledge of the shallow surface of nanodiamonds is required to deeply understand their unusual colloidal properties and reactivity under illumination (radiolysis, $H_2$ production by water splitting, *etc.*). The present study reported on synchrotron X-ray photoemission measurements performed on isolated (or slightly aggregated) NDs in an aerodynamic jet. Under our experimental conditions (a photon energy of 360 eV), the probed depth was 0.3 nm. Using this original configuration, possible charging effects related to the substrate or *in situ* modification of NDs under the photon incident beam can be excluded. First, the synchrotron XPS data allowed us to build band diagrams for oxidized and hydrogenated milled nanodiamonds (Ox-MNDs and H-MNDs). As expected, a negative electron affinity (NEA) was obtained for H-MNDs, whereas the affinity turned positive for Ox-MNDs. Such behaviors are the fingerprint of well-controlled diamond terminations, as shown in the literature. Surprisingly, Ox-MNDs and H-MNDs exhibited quite similar C 1s and O 1s core level signatures, with high oxidized contributions compared to conventional XPS (close to 40% of the C 1s area). If it was rather expected for Ox-MNDs, it is intriguing for the hydrogenated surface, which evidences the NEA at the same time. As a possible explanation for this contradiction, we postulate either a different spatial location of C–O bonds at both MND surfaces, the role

 

of an adsorbed water layer remaining on H-MNDs or the presence of carbon-based adsorbates on the H-MND surface. The contribution of adventitious carbon cannot be completely excluded as well.

Whatever the origin of these unexpected C 1s XPS signatures, synchrotron X-ray photoemission performed on these isolated particles in a jet revealed that hydrogenated and oxidized milled nanodiamonds finally exhibit very similar shallow surface chemistries, despite exhibiting opposite electron affinities. This raises questions concerning the true interface formed with water molecules when MNDs are dispersed in an aqueous suspension, particularly in light of the growing body of research on their use as strong reductive photocatalysts.

## 5. Methods

### Materials

Milled nanodiamonds (SYP 0–0.05, purity >99.9%) were obtained from Van Moppes (Switzerland).

### ND preparation

Oxidized (Ox-MND) and hydrogenated (H-MND) nanodiamond colloids were prepared following the procedure detailed here.[10] In summary, oxidation was conducted by annealing the as-received MNDs (300 mg) at 480 °C for 5 h in air at atmospheric pressure. For hydrogenation, 150 mg of Ox-MNDs was annealed at 750 °C under pure $H_2$ with a flow of 50 sccm at atmospheric pressure. Then, 100 mg of treated powder was sonicated for 30 min in 2.5 mL of ultrapure water (18.2 MΩ cm) using a Cup Horn Bioblock Scientific 750 W system equipped with a cooling system. After a final centrifugation step (40 min at 2400*g*), colloids of H-MNDs and Ox-MNDs were collected and their concentration was measured by weighing the residue of a known volume dried overnight at room temperature.

### Infrared spectroscopy

IR spectra of all samples were obtained using a Bruker Alpha II spectrometer, with 2 μL of suspension drop-casted and dried under $N_2$ on a Platinum ATR system. They reveal the characteristic signatures of oxidized and hydrogenated surfaces with C=O and C–H stretching modes, respectively (Fig. 9). For more details, please refer to our previous studies.[10,18]

### Conventional XPS

The XPS analyses presented here, conducted using a conventional laboratory spectrometer, were derived from our previous study on the same nanoparticles.[10] Briefly, NDs were drop-casted on a silicon substrate covered with a gold coating. Measurements were performed using a Kratos Analytical Axis Ultra DLD spectrometer equipped with a monochromatic Al Kα (1486.6 eV) X-ray source and a charge compensation system (Manchester, UK). The C 1s spectra shown in this study were obtained at a pass energy of 10 eV to achieve a high energy resolution. Binding energies were referenced to the $Au_{4f7/2}$ peak located at 84 eV.

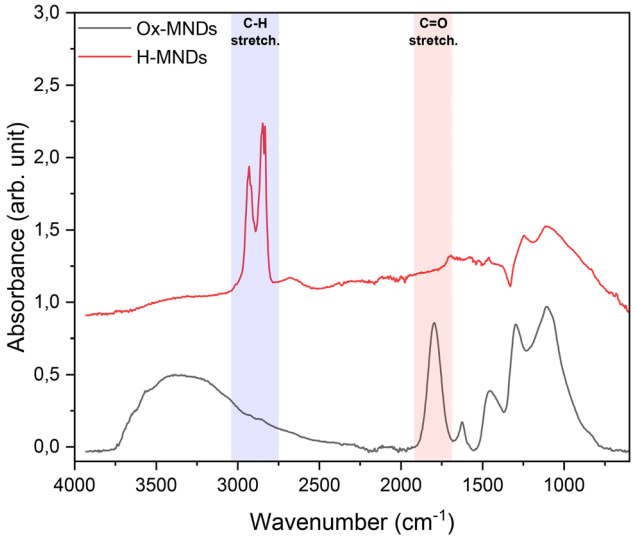


Fig. 9 IR spectra of H-MNDs and Ox-MNDs.

### Jet of nanodiamonds and synchrotron XPS

An aerosol flow composed of an Ar inert carrier gas and the sample in a micro-droplet form was produced by atomization of a suspension of nanoparticles, using a commercial aerosol generator: Palas AGK 2000. The droplets were then dried with a double-stage silica gel dryer from TSI. The aerosol containing dried particles was then driven to an aerodynamic lens system that produces a focused, continuously renewable, nanoparticle beam under vacuum from the aerosol stream at atmospheric pressure. This was achieved by carrying the nano-aerosol flow through a 200 μm limiting entrance orifice, followed by a series of four compartments separated by diaphragms. The geometry of the system is identical to the design previously used on the PLEIADES beamline.[26,45] It is part of a dedicated multipurpose source chamber and the system for X-ray aerosol photoelectron spectroscopy (XAPS)[45] available on the PLEIADES beamline at the French national synchrotron radiation facility SOLEIL.

The nanoparticle beam passes entirely through a 1.5 mm diameter skimmer and emerges into a high vacuum region before crossing the soft X-ray beam. The pressure in the interaction chamber was maintained at around $1 \times 10^{-6}$ mbar. The beam of isolated nanoparticles crosses the synchrotron radiation beam, so that the interaction region between a nanoparticle and soft X-ray photons is well defined spatially. It should be noted that the focused NP beam allows the XPS signal related to the photoionization of NPs to be distinguished from that originating from small atoms/molecules such as the carrier gas, the residual solvent or the gas introduced for calibration.[45]

XPS spectra were recorded using a wide-angle lens VG-Scienta R4000 electron energy analyzer at several different

photon energies, depending on the desired ionization energy (valence or inner shell). The photon beam was produced by a permanent magnet (APPLE II type undulator) with an 80 mm period and monochromatized using a modified Petersen plane grating monochromator and a high-flux 600 L $mm^{-1}$ grating. For the photon energy calibration, the calibration gas was introduced into the calibration chamber (downstream of the XPS measurements) using an effusive jet crossing at the right angle of the SR beam and photo-ions were extracted and detected using a single channel multiplier ("Dr Sjuts Optotechnik GmbH") connected to pulse counting electronics. The overall accuracy of the photon energy calibration in the whole energy range was estimated to be 0.2 eV, not including the accuracy of the literature values used as reference points.

For the photon energies used of 100 eV, 360 eV and 580 eV, the overall resolution in the XPS spectra was 0.11, 0.39, and 0.77 eV, respectively. The linearity of the photoelectron kinetic energy scale was calibrated according to the 2p Ar IPs[55] measured using a Scienta XPS spectrometer under the same experimental conditions. The binding energy (BE) scale with respect to the vacuum level of each particular recorded XPS spectrum was calibrated according to a closely lying XPS line that corresponds to the ionization energy (IE) of an appropriate reference gas. The valence region was calibrated with respect to the ionization energy of water at 12.62 eV (from NIST Chemistry Webbook). The C 1s XPS spectra were calibrated according to the $CO_2$ C 1s IP at 297.7 eV.[31] Note that an uncertainty in the incident photon energy does not influence the calibration of the binding energy scale, which only depends on the uncertainty in the linearity of the photoelectron kinetic energy scale and the error of the reference value. The residual water molecules from the solvent were always present in the interaction region, while calibrant gases (Ar and $CO_2$) were introduced into the chamber through a side leak. The overall uncertainty of BE due to the calibration was estimated to be 0.1–0.2 eV.

## Conflicts of interest

There are no conflicts to declare

## Data availability

Due to the large volume of data collected at the synchrotron, the data will be provided upon request from the authors.

## Acknowledgements

The experiments were performed at the PLEIADES beamline at the SOLEIL Synchrotron, France (Proposal No. 20201236 and 20220294). We thank SOLEIL staff for the expert operation of the equipment and the storage ring during the experiments. The authors also acknowledge J. Leroy from NIMBE for conventional XPS measurements and CEA for funding M. Finas's and L. Saoudi's PhD degrees.

## References

1 H. Wang and Y. Cui, *Carbon Energy*, 2019, **1**, 13–18.
2 Y. Wu and T. Weil, *Adv. Sci.*, 2022, **9**, 1–19.
3 K. P. Loh, D. Ho, G. N. C. Chiu, D. T. Leong, G. Pastorin and E. K. Chow, *Adv. Mater.*, 2018, **30**, 1–21.
4 K. G. Crawford, I. Maini, D. A. Macdonald and D. A. J. Moran, *Prog. Surf. Sci.*, 2021, **96**, 100613.
5 D. Miliaieva, A. S. Djoumessi, J. Čermák, K. Kolářová, M. Schaal, F. Otto, E. Shagieva, O. Romanyuk, J. Pangrác, J. Kuliček, V. Nádaždy, S. Stehlik, A. Kromka, H. Hoppe and B. Rezek, *Nanoscale Adv.*, 2023, **5**, 4402–4414.
6 J. R. Christianson, D. Zhu, R. J. Hamers, J. R. Schmidt, R. Christianson, D. Zhu, R. J. Hamers and J. R. Schmidt, *J. Phys. Chem. B*, 2013, **2**, 195–203.
7 L. Zhang and R. J. Hamers, *Diamond Relat. Mater.*, 2017, **78**, 24–30.
8 W. A. Maza, V. M. Breslin, T. I. Feygelson, P. A. DeSario, B. B. Pate, J. C. Owrutsky and A. Epshteyn, *Appl. Catal., B*, 2023, **325**, 122306.
9 G. Liu, C. Feng and P. Shao, *Environ. Sci. Technol.*, 2022, **56**, 6223–6231.
10 L. Saoudi, H. A. Girard, E. Larquet, M. Mermoux, J. Leroy and J. C. Arnault, *Carbon*, 2023, **202**, 438–449.
11 C. Njel, H. A. Girard, M. Frégnaux, D. Aureau and J.-C. Arnault, *Carbon*, 2024, **230**, 119668.
12 S. Stehlik, O. Szabo, E. Shagieva, D. Miliaieva, A. Kromka, Z. Nemeckova, J. Henych, J. Kozempel, E. Ekimov and B. Rezek, *Carbon Trends*, 2024, **14**, 100327.
13 J. C. Arnault and H. A. Girard, *Curr. Opin. Solid State Mater. Sci.*, 2017, **21**, 10–16.
14 T. Petit, L. Puskar, T. Dolenko, S. Choudhury, E. Ritter, S. Burikov, K. Laptinskiy, Q. Brzustowski, U. Schade, H. Yuzawa, M. Nagasaka, N. Kosugi, M. Kurzyp, A. Venerosy, H. Girard, J.-C. Arnault, E. Osawa, N. Nunn, O. Shenderova and E. F. Aziz, *J. Phys. Chem. C*, 2017, **121**, 5185–5194.
15 K. A. Laptinskiy, A. N. Bokarev, S. A. Dolenko, I. L. Plastun, O. E. Sarmanova, O. A. Shenderova and T. A. Dolenko, *J. Raman Spectrosc.*, 2019, **50**, 387–395.
16 M. Kurzyp, H. A. Girard, Y. Cheref, E. Brun, C. Sicard-Roselli, S. Saada and J.-C. Arnault, *Chem. Commun.*, 2017, **53**, 1237–1240.
17 E. Brun, H. A. Girard, J. C. Arnault, M. Mermoux and C. Sicard-Roselli, *Carbon*, 2020, **162**, 510–518.
18 F. Ducrozet, E. Brun, H. A. Girard, J. C. Arnault and C. Sicard-Roselli, *J. Phys. Chem. C*, 2023, **127**, 19544–19553.
19 C. Marchal, L. Saoudi, H. A. Girard, V. Keller and J. Arnault, *Adv. Energy Sustainability Res.*, 2024, **5**, 1–8.
20 J. C. Arnault, *Diamond Relat. Mater.*, 2018, **84**, 157–168.
21 D. R. Baer and M. H. Engelhard, *J. Electron Spectrosc. Relat. Phenom.*, 2010, **178–179**, 415–432.

 

22 A. G. Shard, J. Wang and S. J. Spencer, *Surf. Interface Anal.*, 2009, **41**, 541–548.
23 A. G. Shard, *J. Phys. Chem. C*, 2012, **116**, 16806–16813.
24 C. Saucedo, N. Rieders and R. J. Hamers, *Diamond Relat. Mater.*, 2025, 112011.
25 M. K. Kuntumalla, A. Chemin, M. Finas, H. A. Girard, S. Michaelson, T. Petit, J.-C. Arnault and A. Hoffman, *J. Phys. Chem. C*, 2024, **128**, 15573–15582.
26 F.-X. Ouf, P. Parent, C. Laffon, I. Marhaba, D. Ferry, B. Marcillaud, E. Antonsson, S. Benkoula, X.-J. Liu, C. Nicolas, E. Robert, M. Patanen, F.-A. Barreda, O. Sublemontier, A. Coppalle, J. Yon, F. Miserque, T. Mostefaoui, T. Z. Regier, J.-B. A. Mitchell and C. Miron, *Sci. Rep.*, 2016, **6**, 36495.
27 S. Benkoula, O. Sublemontier, M. Patanen, C. Nicolas, F. Sirotti, A. Naitabdi, F. Gaie-Levrel, E. Antonsson, D. Aureau, F.-X. Ouf, S.-I. Wada, A. Etcheberry, K. Ueda and C. Miron, *Sci. Rep.*, 2015, **5**, 15088.
28 R.-Q. Yan, M. Cao and Y.-D. Li, *Materials*, 2022, **15**, 3315.
29 S. Tanuma, C. J. Powell and D. R. Penn, *Surf. Interface Anal.*, 2011, **43**, 689–713.
30 H. A. Girard and J.-C. Arnault, in *Novel Aspects of Diamond II*, ed. S. Mandal and N. Yang, Springer Nature Switzerland, Cham, 2024, vol. 149, pp. 47–76.
31 V. Myrseth, J. D. Bozek, E. Kukk, L. J. Sathre and T. D. Thomas, *J. Electron Spectrosc. Relat. Phenom.*, 2002, **122**, 57–63.
32 A. Kahn, *Mater. Horiz.*, 2016, **3**, 7–10.
33 S. Kono, T. Kageura, Y. Hayashi, S. G. Ri, T. Teraji, D. Takeuchi, M. Ogura, H. Kodama, A. Sawabe, M. Inaba, A. Hiraiwa and H. Kawarada, *Diamond Relat. Mater.*, 2019, **93**, 105–130.
34 R. Graupner, J. Ristein and L. Ley, *Surf. Sci.*, 1994, **320**, 201–207.
35 O. Romanyuk, Š. Stehlík, J. Zemek, K. Aubrechtová Dragounová and A. Kromka, *Nanomaterials*, 2024, **14**, 590.
36 K. Kolarova, I. Bydzovska, O. Romanyuk, E. Shagieva, E. Ukraintsev, A. Kromka, B. Rezek and S. Stehlik, *Diamond Relat. Mater.*, 2023, **134**, 109754.
37 S. Stehlik, M. Mermoux, B. Schummer, O. Vanek, K. Kolarova, P. Stenclova, A. Vlk, M. Ledinsky, R. Pfeifer, O. Romanyuk, I. Gordeev, F. Roussel-Dherbey, Z. Nemeckova, J. Henych, P. Bezdicka, A. Kromka and B. Rezek, *J. Phys. Chem. C*, 2021, **125**, 5647–5669.
38 O. S. Kudryavtsev, R. H. Bagramov, A. M. Satanin, A. A. Shiryaev, O. I. Lebedev, A. M. Romshin, D. G. Pasternak, A. V. Nikolaev, V. P. Filonenko and I. I. Vlasov, *Nano Lett.*, 2022, **22**, 2589–2594.
39 E. Ekimov, A. A. Shiryaev, Y. Grigoriev, A. Averin, E. Shagieva, S. Stehlik and M. Kondrin, *Nanomaterials*, 2022, **12**, 1–22.
40 D. R. Baer, M. H. Engelhard, G. E. Johnson, J. Laskin, J. Lai, K. Mueller, P. Munusamy, S. Thevuthasan, H. Wang, N. Washton, A. Elder, B. L. Baisch, A. Karakoti, S. Kuchibhatla and D. Moon, *J. Vac. Sci. Technol., A*, 2013, **31**, 050820.
41 M. Finas, H. A. Girard and J.-C. Arnault, *Nanoscale Adv.*, 2024, **6**, 5375–5387.
42 O. Sublemontier, C. Nicolas, D. Aureau, M. Patanen, H. Kintz, X. Liu, M.-A. Gaveau, J.-L. Le Garrec, E. Robert, F.-A. Barreda, A. Etcheberry, C. Reynaud, J. B. Mitchell and C. Miron, *J. Phys. Chem. Lett.*, 2014, **5**, 3399–3403.
43 A. Chemin, M. K. Kuntumalla, M. Brzhezinskaya, T. Petit and A. Hoffman, *Appl. Surf. Sci.*, 2024, **661**, 160082.
44 P. Wang, T. X. Carroll, T. D. Thomas, L. J. Sæthre and K. J. Børve, *J. Electron Spectrosc. Relat. Phenom.*, 2021, **251**, 147103.
45 D. Danilović, D. K. Božanić, R. Dojčilović, N. Vukmirović, P. Sapkota, I. Vukašinović, V. Djoković, J. Bozek, C. Nicolas, S. Ptasinska and A. R. Milosavljević, *J. Phys. Chem. C*, 2020, **124**, 23930–23937.
46 D. Cahen and A. Kahn, *Adv. Mater.*, 2003, **15**, 271–277.
47 O. Manelli, S. Corni and M. C. Righi, *J. Phys. Chem. C*, 2010, **114**, 7045–7053.
48 A. Laikhtman, A. Lafosse, Y. Le Coat, R. Azria and A. Hoffman, *Surf. Sci.*, 2004, **551**, 99–105.
49 R. Akhvlediani, S. Michaelson and A. Hoffman, *Surf. Sci.*, 2010, **604**, 2129–2138.
50 F. Maier, M. Riedel, B. Mantel, J. Ristein and L. Ley, *Phys. Rev. Lett.*, 2000, **85**, 3472–3475.
51 M. Riedel, J. Ristein and L. Ley, *Phys. Rev. B:Condens. Matter Mater. Phys.*, 2004, **69**, 125338.
52 C. Yang, F. Bebensee, J. Chen, X. Yu, A. Nefedov and C. Wöll, *ChemPhysChem*, 2017, **18**, 1874–1880.
53 G. Greczynski and L. Hultman, *ChemPhysChem*, 2017, **18**, 1507–1512.
54 G. Greczynski and L. Hultman, *Appl. Surf. Sci.*, 2018, **451**, 99–103.
55 A. Thompson, D. Attwood, E. Gullikson, M. Howells, K.-J. Kim, J. Kirz, J. Kortright, I. Lindau, Y. Liu, P. Pianetta, A. Robinson, J. Scofield, J. Underwood, G. Williams and H. Winick, X-Ray Data Booklet, Lawrence Berkeley National Laboratory, 2009.